IOP Publishing | Royal Swedish Academy of Sciences Physica Scripta

Phys. Scr. **T170** (2017) 014009 (6pp) https://doi.org/10.1088/1402-4896/aa8784

Cracking and surface roughening of beryllium–tungsten alloy due to transient heating

J H Yu, M J Baldwin and R P Doerner

Center for Energy Research, University of California, San Diego, La Jolla, CA 92093-0417, United States of America

E-mail: j2yu@eng.ucsd.edu

Received 26 May 2017, revised 11 August 2017
Accepted for publication 22 August 2017
Published 13 September 2017

Abstract

A controlled beryllium–tungsten (Be–W) alloy was created in a beryllium-seeded deuterium plasma in the PISCES-B facility and irradiated by a pulsed laser in order to investigate how transient surface heating from plasma instabilities will affect the performance of mixed materials in ITER. Standardized wavelength dispersive x-ray spectroscopy was used to measure the depth profiles of beryllium and tungsten atomic concentrations, revealing beryllium penetration of $\sim$100 μm in ITER comparable grade tungsten with 5000 s of plasma exposure at 1123 K and ion flux 8×10^{22} m^{-2} s^{-1}. The deep Be penetration into W is a concern for the lifetime of the ITER divertor, which may form mixed Be–W material. Pulsed laser heating was used to investigate the thermo-mechanical response of Be–W alloy and pure W using temporal shape mimicking that expected for edge-localized modes in ITER, with up to 1.9 MJ m^{-2} of absorbed energy density. Transient heating creates a lower surface roughness than pure W, but cracks appear in the alloy layer surface at lower absorbed energy density and lower pulse number.

Keywords: ITER, plasma-material interactions, tungsten, beryllium, laser heating, alloy

(Some figures may appear in colour only in the online journal)

1. Introduction

Transient heat loads on the ITER tungsten (W) divertor due to ELMs, VDEs, and possible disruptions will push the boundaries of material limits. Eroded Be from the first wall will flow in the scrape off layer toward the divertor, and the incident Be on the W divertor may form a Be–W alloy under certain conditions [1–4]. The tungsten beryllide system in equilibrium [5] consists of three alloys (Be_2W, $Be_{12}W$, and $Be_{22}W$), all of which have a lower melting temperature than pure tungsten. In previous work the response of pure W [6–9] and pure Be [10, 11] to transient heat loads has been investigated in detail, but the response of mixed Be–W surfaces to transient heating events has not been well studied. The formation of Be–W alloy has been previously shown to occur due to laser heating of Be-coated W [12], raising the possibility that Be–W alloy will form in the ITER divertor during ELM heating even if the steady state divertor temperature is insufficient. However, other work showed that transient heating can exceed the ablation threshold of Be in co-deposited layers [13], and in ITER a competition is expected between the arrival rate of Be at the W surface which can cause alloying at elevated temperature, and its sublimation and erosion. In the present work, a Be–W alloy was formed on ITER grade W under controlled steady state conditions using the PISCES-B plasma facility. The plasma was then turned off and the influence of repetitive transient heating on surface roughness and cracking for both the mixed and pure W surfaces was investigated.

2. Experimental setup

A polished ITER grade W sample (Midwest Tungsten) with diameter 25 mm and thickness 2 mm was exposed to Be-seeded D plasma in the PISCES-B facility [14] with sample temperature 1123 K, plasma flux 8×10^{22} m^{-2} s^{-1}, ion energy $\sim$10 eV, and

$n_{Be}{}^{+}/n_e$ approximately 0.003. After 5000 s the flux of Be was stopped, and D plasma was continued for additional 1000 s in order to erode any remaining Be on the sample surface, leaving a clean alloy surface for subsequent laser heating.

Following plasma exposure, thermal shock testing was performed using a pulsed Nd:YAG laser with wavelength of 1064 nm, maximum absorbed power density of $\sim$2 GW m^{-2}, approximately Gaussian spatial profile, programmable pulse shape, and incident angle of 15° with respect to the sample normal. For most data shown here, the laser was programmed to create a temporal pulse shape similar to the estimated shape predicted for type-I ELMs in ITER [15], with rise time of 0.25 ms, total pulse width of 1 ms, and energy density ranging from 0.4 to 0.8 MJ m^{-2}. Longer pulse widths up to 2.3 ms were used to achieve transient heating with higher total energy density up to 1.9 MJ m^{-2}. The laser pulse repetition frequency was 0.2 Hz, allowing the sample to cool to the base temperature of $<$310 K between laser pulses as measured by a thermocouple on the back side of the sample. For each type of heat pulse, a reference tungsten sample that received no plasma exposure was irradiated by the laser. The measured optical specular reflectivities of the Be–W surface and the reference W sample were taken into account in order to adjust the laser intensity to produce the same absorbed heat flux on both samples.

Both the Be–W alloy and W samples were analyzed with a confocal microscope (CM) and scanning electron microscope (SEM) to assess transient heat-induced surface damage. The Be–W sample was also analyzed using standardized wavelength dispersive x-ray spectroscopy (WDS) and energy dispersive x-ray spectroscopy. The surface roughness in the laser irradiated areas was measured with the CM along line profiles through the center of the laser spot extending to the edge of the damaged area. We report here the average roughness R_a, which is defined as the arithmetic average of the absolute values of the surface height deviations relative to the mean height.

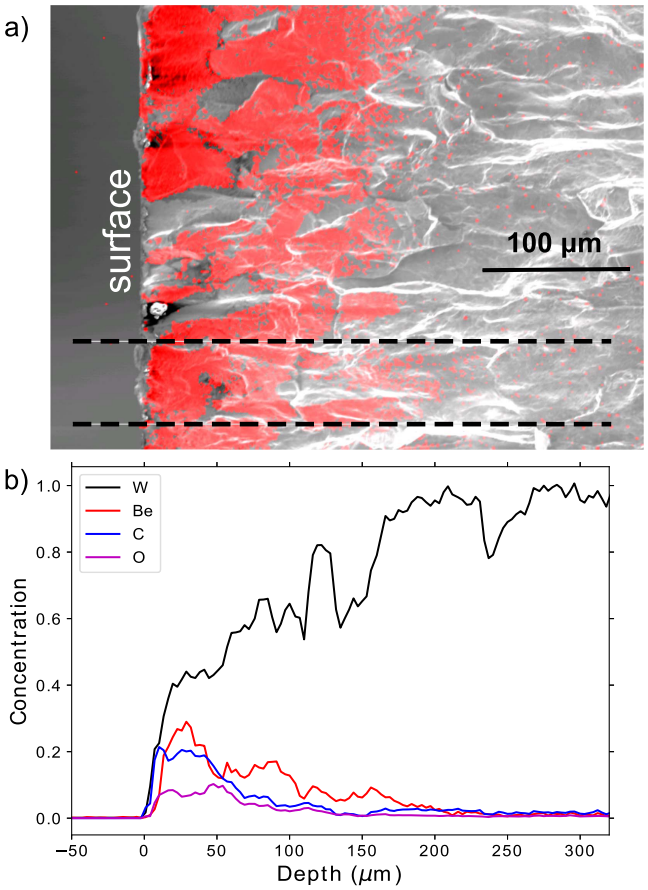

Figure 1. (a) WDS mapping of Be (shown in red) overlaid on an SEM image of the Be–W sample cross-section. The concentration profiles shown in (b) are calculated from the average of the depth profiles located between the dashed lines in (a).

3. Results

3.1. Be–W alloy formation

The plasma conditions and sample temperature during plasma exposure were chosen to create a $\sim$1 μm Be–W alloy layer based on the work done in [1], which used W with grain orientation parallel to the sample surface (despite being described as ITER grade). Surprisingly, for the W samples studied here with grains oriented perpendicular to the sample surface, beryllium penetrated much deeper than expected and reached depth of $\sim$100 μm, as shown in the standardized WDS Be mapping of the cross section in figure 1(a). The depth profile of beryllium shown in figure 1(b) was obtained from WDS analysis of the sample cross section, while the profiles for tungsten, carbon, and oxygen were obtained by EDX analysis, with the concentrations normalized to standardized WDS measurements of these elements at a depth of $\sim$25 μm. The peak Be atomic concentration was 0.3, while the peak concentrations for carbon and oxygen were smaller, but their overall profile shapes were similar to that of Be due to carbon contamination and formation of BeO. The deep Be penetration in ITER grade W indicates that Be can easily diffuse along grain boundaries at elevated temperature, and raises a potential concern for the ITER divertor due to embrittlement of the alloy layer.

3.2. Optical reflectivity

The optical specular reflectivity of the W and the Be–W samples was measured in order to adjust the laser intensity to provide similar absorbed heat fluxes on each sample for each set of laser conditions. The reflectivity measurements were made in the wavelength range from 400 to 1030 nm using an Ocean Optics USB2000 spectrometer viewing the sample surface at an angle of approximately 10° with respect to the sample normal. An objective lens collected light along a collimated viewing chord, and photons were guided to the spectrometer using a fiber optic cable. A calibrated integrating sphere was used as the light source and provided spatially uniform light intensity in the visible to the near infrared spectrum. The reflectivity was determined from the ratio of

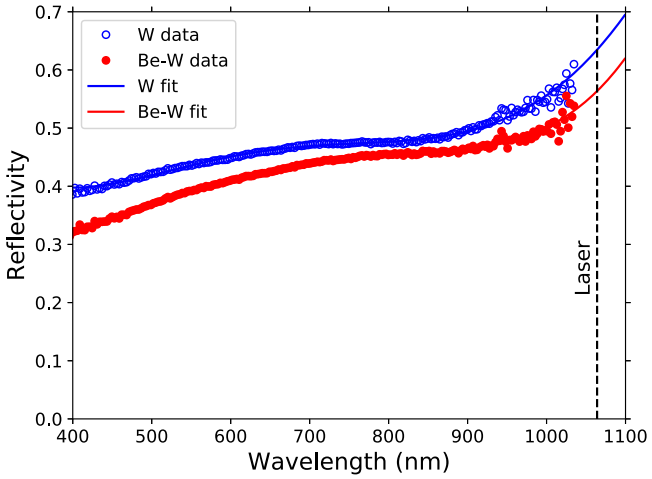

Figure 2. Optical specular reflectivity measurements and polynomical fits for the Be–W and pure W surfaces before laser heating.

the measured reflected light, $I_r(\lambda)$, to the intensity of the source light, $I_o(\lambda)$, with the background ambient light $I_b(\lambda)$ subtracted, i.e.,

$$R(\lambda) = \frac{I_r(\lambda) - I_b(\lambda)}{I_o(\lambda) - I_b(\lambda)}.$$

Figure 2 shows that the reflectivity of the Be–W mixed material surface was 5%–20% lower than W over the visible spectral range. The reflectivity measurements were fit with polynomials and extrapolated to the laser wavelength of 1064 nm, resulting in reflectivities of 0.56 and 0.63 for the mixed Be–W surface and W, respectively.

3.3. Transient heating

The samples were irradiated by the laser with ELM-like temporal pulse shape and $1/e^2$ spot size diameter of $\sim$500 μm. For each set of laser conditions, the absorbed heat flux factor, $F = E/\sqrt{\tau}$, was kept the same for both the Be–W and the W samples in order to provide similar heating by adjusting the laser intensity to account for the difference in sample reflectivities, where E is the absorbed energy density and τ is the total pulse width. For example, using the same pulse width, the incident laser intensity ($P^{\rm in}_{\rm BeW}$) for the mixed material sample was programmed to be lower than that ($P^{\rm in}_{\rm W}$) for tungsten, i.e., $\frac{P^{\rm in}_{\rm BeW}}{P^{\rm in}_{\rm W}} = \frac{1-0.63}{1-0.56} = 0.84$. In previous work [7] it was shown that F is a misleading metric when comparing different temporal pulse shapes such as ELM-like and rectangular. However, for self-similar pulse shapes (same ratio of rise time to total pulse width), F can be used as a relative measure of the surface temperature rise, provided the thermomechanical properties are the same.

Laser-induced damage is seen on the mixed material surface (figures 3(a)–(c)) and the pure tungsten surface (figures 3(d)–(f)) for pulse numbers of 10, 100, and 500 using the same pulse shape and approximately the same absorbed energy density. The absorbed power densities in figure 3(g) represent the initial laser pulses and do not take into account changes to the reflectivity due to surface roughening. The observed damage was qualitatively similar for the two types of samples, but significant differences exist including cracks that occur at lower pulse number in the mixed material, as well as the appearance of secondary cracks in Be–W. The primary cracks were oriented in an annular pattern where thermal gradients were large, and cracking was caused by tensile stresses during cooling. In other laser spots with different temporal pulse shapes, a random crack pattern was visible in the center of the spot (not shown here). Most of those laser pulses had a faster decrease of laser power at the end of the pulse, and thus a faster cooling time. Further study is needed to establish a definitive correlation between crack pattern and cooling time.

The surface temperature was measured with a 2-color pyrometer [7], as shown in figure 3(h). The ratio technique used for pyrometer analysis in principle calculates the highest surface temperature within the laser spot, and the main source of error was the large pyrometer viewing spot (20 mm) compared to the laser spot (0.5 mm). This error was systematic, but the repeatability was sufficiently good that the differences between the measured surface temperatures from the two samples were significant. The surface temperature rise of the Be–W sample was slightly lower than that of the W sample. This difference in thermal response is attributed to different thermomechanical properties of the two sample surfaces and indicates that the product cK, where c is the specific heat and K is the thermal conductivity, is larger for Be–W compared to W (assuming that the density ρ for the mixed layer is lower than that for pure W). This is inferred from the fact that for a given pulse shape the surface temperature rise ΔT scales with $F(K\rho c)^{-1/2}$. In addition, the peak surface temperature during laser heating increased as a function of pulse number (also observed in [16, 17]), as seen by comparing the solid and dashed curves in figure 3(h). This increase is not attributed to an increase in the base temperature, which was monitored by a thermocouple, but rather to an increase in surface roughness which caused the optical reflectivity to decrease, resulting in higher absorbed laser power. The increase in peak surface temperature with pulse number is also attributed to progressive degradation of heat conduction in the damaged layer.

Following laser irradiation, the surface roughness $R_{\rm a}$ was measured using a CM. Surface roughness occurs due to the cumulative plastic deformation of the material near the surface, and with repeated cycling $R_{\rm a}$ increases due to the repeated movement of dislocations caused by thermal expansion during heating and contraction during cooling. The surface roughness of Be–W was lower than that of W for similar absorbed transient heat loads, as seen in figures 4(a) and (b). However, as mentioned, even with lower $R_{\rm a}$ the alloy was observed to crack more readily than W, with crack initiation at lower peak surface temperature, lower pulse number, and larger maximum crack width, as shown in figure 4(c). One question that might arise is the influence of plasma exposure on crack formation. Work done using electron beam heating in [18] showed that tungsten preloaded with high flux hydrogen plasma had lower crack widths, smaller crack penetration depths, and higher crack densities compared to unloaded tungsten. The larger crack widths

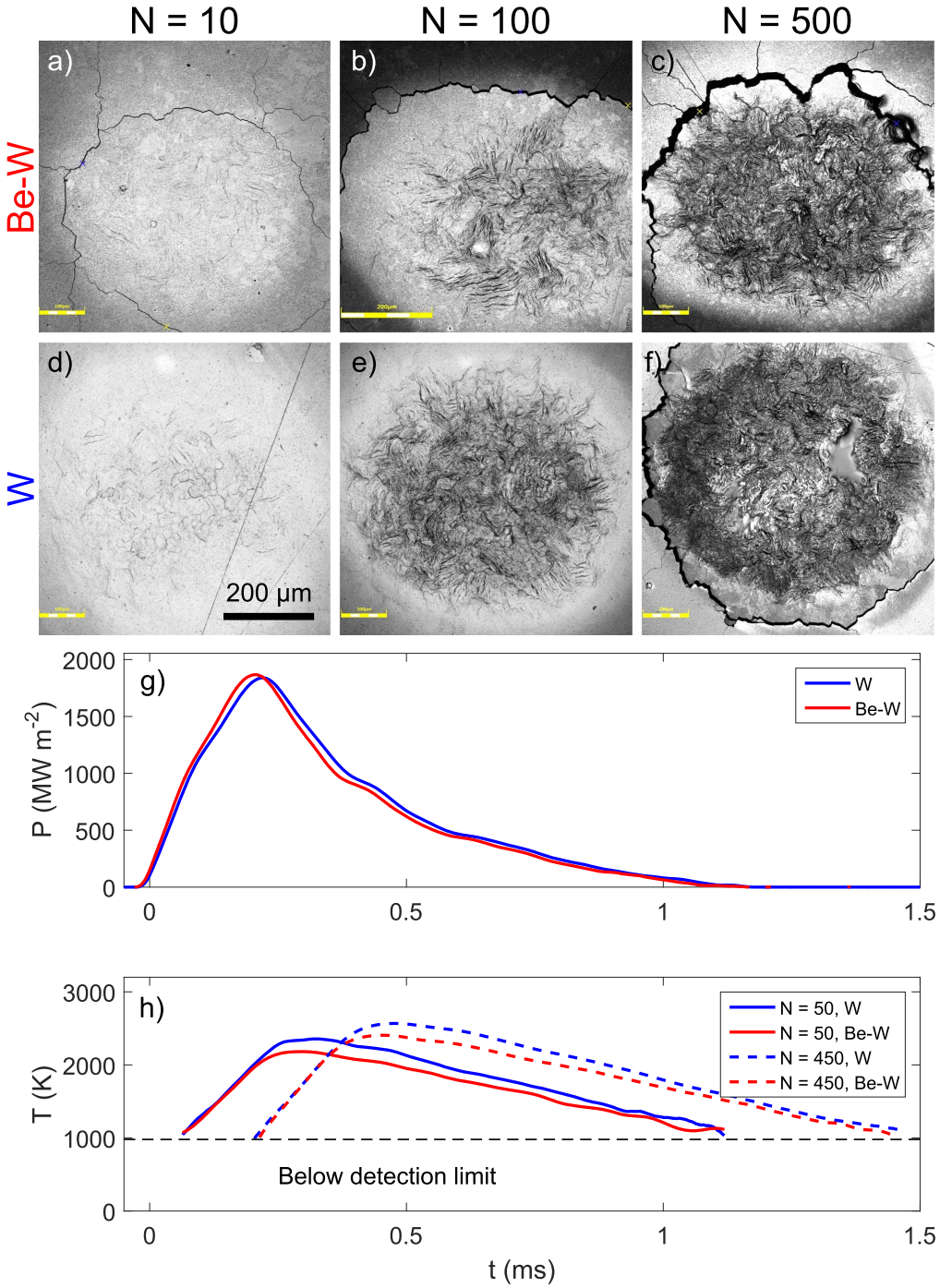

Figure 3. Confocal microscopy images of (a)–(c) Be–W and (d)–(f) pure W with various pulse numbers using initial absorbed energy densities of 0.71 and 0.75 MJ m^{-2} for Be–W and W, respectively. (g) Absorbed laser power densities for initial pulses and (h) measured surface temperature for each sample after 50 pulses (solid) and 450 pulses (dashed). The dashed curves are time delayed for visibility.

observed in our Be/D-exposed samples suggest that embrittlement due to alloying is the dominant reason for enhanced cracking, as opposed to deuterium embrittlement.

Much higher heat loads using disruption-like heat flux factor of 235 MJ m^{-2} s$^{-1/2}$, 10 ms pulse width, and approximately rectangular temporal pulse shape, were also applied to both samples resulting in a melt crater in the laser irradiated area and recrystallized tungsten. Interestingly, SEM imaging following a single disruption-like heat pulse on the mixed Be–W sample revealed micron-sized particles were ejected from the laser spot which created a debris field visible up to a few hundred microns from the edge of the laser irradiated area, as seen in figure 5. No debris was visible on the pure W sample. The number density of the particles in the debris field depended on the distance from the laser spot, with low density near the edge of the laser spot, and peak density located approximately 300 μm from the edge. The thermal shock-induced ejection of particles presumably occurred due to the loss of ductility of the near-surface mixed-material.

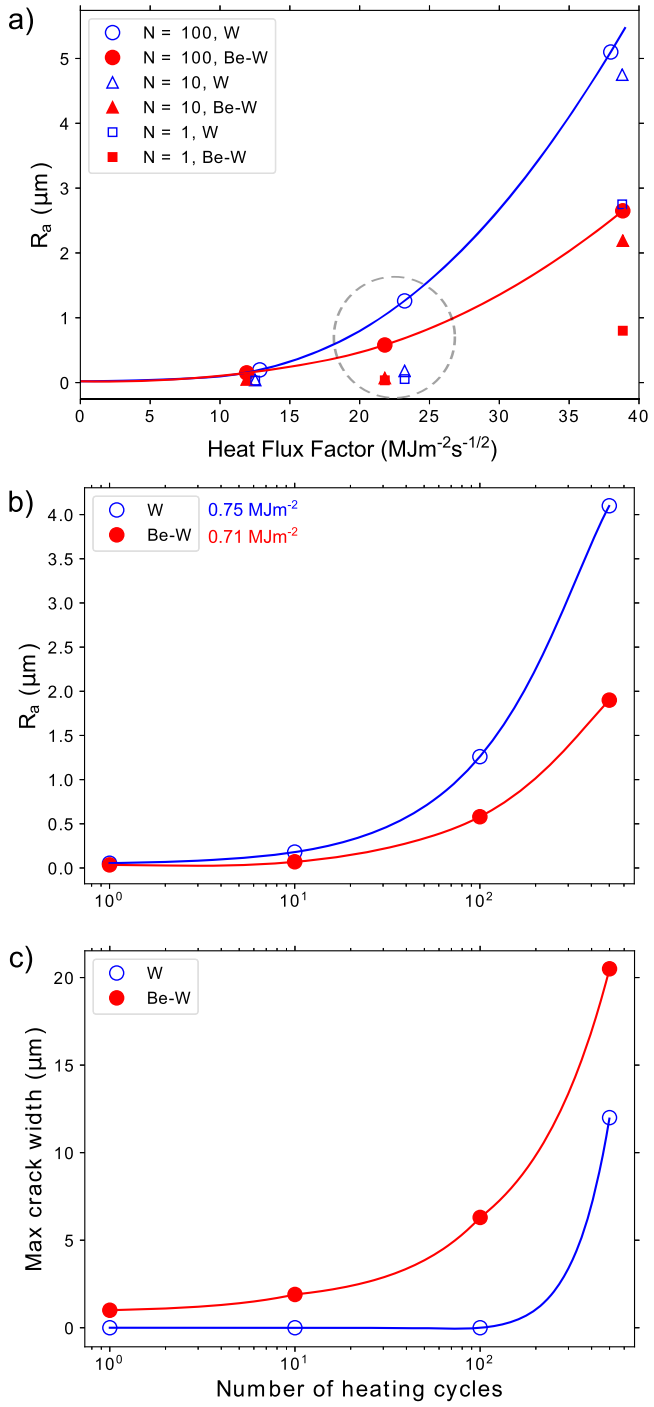

Figure 4. (a) Arithmetic average surface roughness R_a versus the heat flux factor defined in terms of the absorbed energy density and total pulse width. The dashed circle shows the data (except for the $N = 500$ case) displayed in (b) and (c).

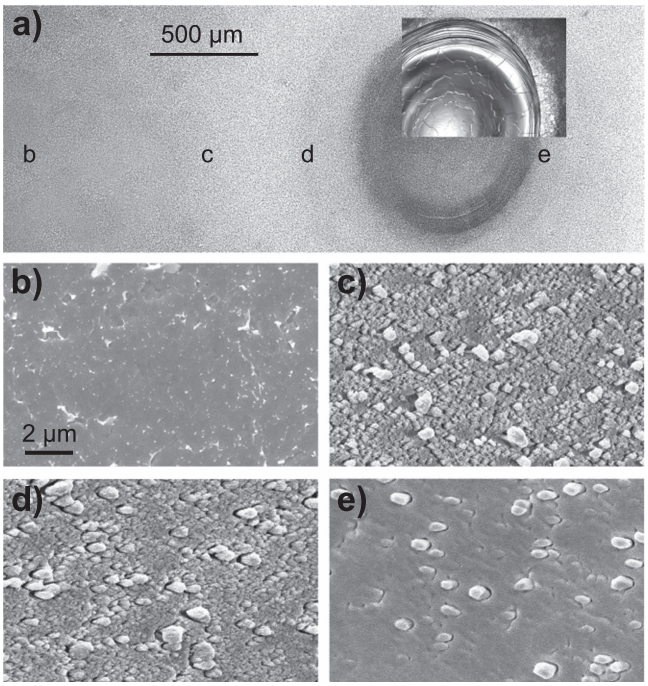

Figure 5. (a) SEM image of the laser irradiated spot and surrounding area after a single disruption-like heat pulse with duration 10 ms and heat flux factor of 235 MJ m^{-2} s$^{-1/2}$. The partial inset shows a more detailed view of the recrystallized melted area from a confocal microscope. The letters correspond to the locations of the higher magnification SEM images in (b)–(e). The thermal shock-induced debris is visible in (c)–(e); an image with no debris is shown in (b).

4. Discussion and conclusions

Modeling [19, 20] has predicted that a Be layer can develop on the divertor at the rate of up to 1 nm s^{-1}, but the question of Be–W alloy formation in the ITER divertor is still open. At low surface temperature, diffusion is low and so any alloying will be limited. Baldwin [1] has shown that the formation of an alloy requires sufficient Be at the W surface, and if the surface temperature is large, sublimation limits the amount of Be available. If the arrival rate is high enough then a higher temperature is needed to remove Be in order to prevent alloy formation. In addition, erosion will limit the available Be, so alloying depends on the interplay between surface temperature, Be arrival rate, sublimation, and erosion. The deep Be penetration of $\sim$100 μm observed here for ITER grade W is alarming considering the increased embrittlement of the mixed material compared to W occurred after only 5000 s of exposure to Be-seeded plasma.

Changes to the optical and thermomechanical properties of mixed Be–W compared to W were observed. Knowledge of the optical reflectivities of PFCs may be beneficial to optical diagnostics used in future tokamaks, and in the present work the specular optical reflectivity of Be–W was found to be lower than that of W over the visible and near IR spectrum.

Laser heating using ELM-like heating caused a lower surface roughness in the mixed material, but a higher propensity for cracking. Surface roughness is often used as an indication of the severity of surface damage, and typically a threshold roughness is needed in order to observe the onset of cracking. Here we show that the threshold roughness is lower for Be–W compared to W, leading to alloy cracking at lower absorbed energy density and lower peak surface temperature compared to pure W. The higher susceptibility of Be–W mixed material to cracking under transient thermal loads is a concern for the ITER divertor, because cracking can lead to the development of leading edges that receive higher heat

loads than surrounding material. In addition, cracking lowers the effective thermal conductivity.

A single 10 ms laser pulse delivering a disruption-like heat load melted the material over the entire laser spot and recrystallized the near surface region. Post mortem SEM analysis revealed micron-sized particles were ejected from the thermally-damaged area on the Be–W surface, but not on pure W. While material damage during disruption-like heat loads will be of primary concern, the ejected embrittled mixed material would be an obvious source of dust, which will have regulatory limits in ITER.

The results presented here indicate that further careful modeling of the ITER divertor environment is needed, including the formation of mixed Be–W layers due to Be flux from first wall erosion, as well as the response of mixed materials to transient thermal loads. In addition, direct testing of the thermomechanical properties of mixed materials is needed. Future experimental work should include testing different base temperatures including above the ductile to brittle transition temperature, as fracture toughness typically increases with temperature. Other work includes applying transient heating during plasma exposure to determine whether Be is driven further into the material.

Acknowledgments

This work was supported by US DOE grant #DE-FG02-07ER54912.

References

[1] Baldwin M J, Doerner R P, Nishijima D, Buchenauer D, Clift W M, Causey R A and Schmid K 2007 *J. Nucl. Mater.* **365** 1179
[2] Linsmeier C, Ertl K, Roth J, Wiltner A, Schmid K, Kost F, Bhattacharyya S R, Baldwin M and Doerner R P 2007 *J. Nucl. Mater.* **363** 1129
[3] Lipschultz B *et al* 2007 *Nucl. Fusion* **47** 1189
[4] Doerner R P, Baldwin M J and Causey R A 2005 *J. Nucl. Mater.* **342** 63
[5] Okamoto H and Tanner L E 1991 *Phase Diagrams of Binary Tungsten Alloys* (Calcutta: Indian Institute of Metals)
[6] Morgan T W, Zielinski J J, Hensen B J, Xu H Y, Marot L and De Temmerman G 2013 *J. Nucl. Mater.* **438** 784
[7] Yu J H, De Temmerman G, Doerner R P and Pitts R A 2015 *Nucl. Fusion* **55** 093027
[8] Loewenhoff T, Bardin S, Greuner H, Linke J, Maier H, Morgan T W, Pintsuk G, Pitts R A, Riccardi B and De Temmerman G 2015 *Nucl. Fusion* **55** 123004
[9] Klimov N *et al* 2009 *J. Nucl. Mater.* **390** 721
[10] Pintsuk G, Kühnlein W, Linke J and Rödig M 2007 *Fusion Eng. Des.* **82** 1720
[11] Spilker B, Linke J, Pintsuk G and Wirtz M 2016 *Phys. Scr.* **T167** 014024
[12] Yu J H, Doerner R P, Dittmar T, Höschen T, Schwarz-Selinger T and Baldwin M J 2014 *Phys. Scr.* **T159** 014036
[13] Yu J H, Baldwin M J, Doerner R P, Dittmar T, Hakola A, Höschen T, Likonen J, Nishijima D and Toudeshki H H 2015 *J. Nucl. Mater.* **463** 299
[14] Doerner R P, Baldwin M J and Schmid K 2004 *Phys. Scr.* **T111** 75
[15] Eich T, Thomsen H, Fundamenski W, Arnoux G, Brezinsek S, Devaux S, Herrmann A, Jachmich S and Rapp J 2011 *J. Nucl. Mater.* **415** S856
[16] Van Eden G G, Morgan T W, Van der Meiden H J, Matejicek J, Chraska T, Wirtz M and De Temmerman G 2014 *Nucl. Fusion* **54** 123010
[17] Buzi L, De Temmerman G, Huisman A E, Bardin S, Morgan T W, Rasinski M, Pitts R A and Van Oost G 2017 *Nucl. Fusion* (https://doi.org/10.1088/1741-4326/aa81e4) (accepted)
[18] Wirtz M, Linke J, Pintsuk G, De Temmerman G and Wright G M 2013 *J. Nucl. Mater.* **443** 497
[19] Kirschner A, Borodin D, Philipps V, Samm U, Ding R, Schmid K, Roth J, Kukushkin A, Federici G and Loarte A 2009 *J. Nucl. Mater.* **390** 152
[20] Schmid K 2008 *Nucl. Fusion* **48** 105004